

# Langevin DQN

**Vikranth Dwaracherla**

*Stanford University*

VIKRANTH@STANFORD.EDU

**Benjamin Van Roy**

*Stanford University*

BVR@STANFORD.EDU

## Abstract

Algorithms that tackle deep exploration – an important challenge in reinforcement learning – have relied on epistemic uncertainty representation through ensembles or other hypermodels, exploration bonuses, or visitation count distributions. An open question is whether deep exploration can be achieved by an incremental reinforcement learning algorithm that tracks a single point estimate, without additional complexity required to account for epistemic uncertainty. We answer this question in the affirmative. In particular, we develop Langevin DQN, a variation of DQN that differs only in perturbing parameter updates with Gaussian noise, and demonstrate through a computational study that the algorithm achieves deep exploration. We also provide an intuition for why Langevin DQN performs deep exploration.

## 1. Introduction

In reinforcement learning (RL), intelligent exploration relies on decisions that are driven not only by expectations but also epistemic uncertainty. Thompson Sampling (TS), for example, is a popular exploration scheme that makes decisions based on a posterior distribution over models (Thompson, 1933; Russo et al., 2018). In its basic form, to generate decision, TS samples a model from the posterior and then selects an action that optimizes the sampled model.

Generating exact posterior samples is computationally feasible only for very simple environments, like tabular MDPs with Dirichlet priors over transition probability vectors (Osband et al., 2013). Scaling TS to complex domains calls for approximations (Russo et al., 2018). To serve this need, Osband et al. (2019) developed randomized least-squares value iteration (RLSVI), which aims to approximately sample from the posterior over the optimal value function without explicitly representing the distribution. This algorithm randomly perturbs a prior and an accumulated dataset, and fits to this perturbed prior and data a point estimate of the value function. The randomness induced by perturbations induces an intelligent form of exploration in actions subsequently selected to maximize the resulting value estimates.

Though RLSVI avoids maintaining an explicit posterior distribution, for each episode of operation, the algorithm produces a new point estimate based on an independently perturbed data set. This requires intensive computations which do not leverage previously computed point estimates. Ensemble sampling (Osband et al., 2016, 2019; Lu and Van Roy, 2017) can approximate the performance of RLSVI via maintaining a set of point estimates, each updated incrementally as data accumulates. However, maintaining an ensemble of complex models is itself computationally burdensome.

As an alternative to maintaining an ensemble of models, one can instead learn a *hypermodel*, which can be used to generate approximate posterior samples, as discussed in (Dwaracherla et al.,

2019, 2020). This is a promising approach, but it requires a representation that can be much more complex than a point estimate of the value function.

An important feature of RLSVI and incremental variants that leverage ensembles or more general hypermodels is that they exhibit intelligence in the form of *deep exploration*. In particular, actions are taken to resolve epistemic uncertainty not only based on immediate consequences but also what will be observed over the subsequent time periods. In this paper, we seek to understand whether a reinforcement learning algorithm that evolves a single point estimate of the optimal value function through incremental training can achieve deep exploration. We propose an algorithm – Langevin DQN – which we believe to serve this purpose. This algorithm synthesizes DQN (Mnih et al., 2013) and stochastic gradient Langevin iterations (Welling and Teh, 2011).

On the surface, Langevin DQN may appear to share motivation and spirit with the “noisy networks” version of DQN (Fortunato et al., 2018), which randomly perturbs neural network weights both when computing state-action and target values for training and in selecting actions. But there are critical differences as is evidenced by the fact that noisy networks do not achieve deep exploration (Osband et al., 2018).

We provide some background on Langevin Monte Carlo and episodic reinforcement learning problem in Section 2 and 3 respectively. We introduce our proposed Langevin DQN algorithm in Section 4 and follow with computational results that show deep exploration in an environment known as *deep sea* in Section 5. In Section 6, we provide some intuition on why the Langevin DQN algorithm exhibits deep exploration.

## 2. Langevin SGD

Langevin Monte Carlo is a Markov chain Monte-Carlo (MCMC) algorithm that can generate samples approximately from a desired probability distribution. The algorithm represents a discrete-time approximation to the Langevin diffusion process, which takes the form

$$d\bar{\theta}_t = \nabla_{\theta=\bar{\theta}_t} \log p(\theta) dt + \sqrt{2} dB_t,$$

where  $\bar{\theta}_t$  takes values in  $\mathfrak{R}^d$ ,  $p$  is the probability density of interest, and  $B_t$  is a standard Brownian motion in  $\mathfrak{R}^d$ . Under suitable technical conditions, it can be shown that  $p$  is the unique invariant distribution of the Langevin diffusion process (see e.g., Proposition 6.1 in (Pavliotis, 2014)).

A common Langevin Monte Carlo algorithm arises from Euler-Maruyama discretization:

$$\Delta\theta_k = \epsilon_k \nabla_{\theta=\theta_{k-1}} \log p(\theta) + \sqrt{2\epsilon_k} z_k, \tag{1}$$

where  $\Delta\theta_k = \theta_k - \theta_{k-1}$ ,  $\epsilon_k \in \mathfrak{R}_+$  is a step size,  $z_k$  is independently sampled from the  $d$ -dimensional standard normal distribution, and  $\theta_k$  represents an approximation of  $\bar{\theta}_t$  with  $t = \sum_{j=1}^k \epsilon_j$ . The hope is that, under technical regularity conditions and with a suitable step size sequence, for sufficiently large  $k$ , the marginal distribution of  $\theta_k$  is close to  $p$  (for example, non-asymptotic convergence rates with respect to the 1-Wasserstein distance are provided in (Cheng et al., 2018)).

Before we develop Langevin DQN, it is helpful to first discuss a simpler but closely related application of Langevin Monte Carlo, which we will refer to as Langevin SGD. In particular, consider a supervised learning problem, where given a set  $\mathcal{D} = \{(x_i, y_i)\}_{i=1}^T$  of data pairs, each in  $\mathcal{X} \times \mathfrak{R}$ , the goal is to fit a function  $f_\theta : \mathcal{X} \rightarrow \mathfrak{R}$ , which is parameterized by  $\theta \in \mathfrak{R}^d$ . If we assume that  $y_i = f_{\theta^*}(x_i) + w_i$  for some  $\theta^* \in \mathfrak{R}^d$  and iid  $w_i \sim \mathcal{N}(0, \sigma_w^2)$  then the negative log-likelihood function

is given by

$$\mathcal{L}(\theta, \mathcal{D}) = \sum_{i=1}^T \frac{(f_{\theta}(x_i) - y_i)^2}{2\sigma_w^2}$$

Further, letting  $\psi$  denote the prior distribution of  $\theta^*$ , the posterior log-density of  $\theta^*$  is given by

$$\log p(\theta|\mathcal{D}) = -\mathcal{L}(\theta, \mathcal{D}) - \psi(\theta).$$

Specialized to our supervised learning context, the Langevin Monte Carlo algorithm (1) becomes

$$\begin{aligned} \Delta\theta_k &= \epsilon_k \nabla_{\theta=\theta_{k-1}} \log p(\theta|\mathcal{D}) + \sqrt{2\epsilon_k} z_k, \\ &= -\epsilon_k \nabla_{\theta=\theta_{k-1}} (\mathcal{L}(\theta, \mathcal{D}) + \psi(\theta)) + \sqrt{2\epsilon_k} z_k. \end{aligned} \quad (2)$$

This iteration is like gradient descent, but with an extra term that injects noise into the parameter update. Let us refer to this as *Langevin gradient descent*. While gradient descent aims to converge on a MAP estimate of  $\theta^*$ , Langevin gradient descent generates a stochastic sequence of parameter vectors  $\theta_0, \theta_1, \theta_2, \dots$  such that, under suitable technical conditions and for sufficiently large  $k$ , the marginal distribution of  $\theta_k$  offers a close approximation to the posterior distribution of  $\theta^*$ .

When the dataset  $\mathcal{D}$  is large, processing the entire dataset in each iteration may be computationally onerous. It is thus common to use stochastic gradient descent (SGD), which carries out each update step using a minibatch of data, rather than standard gradient descent. Similarly, we can replace each Langevin gradient descent step (2) with one computed from a minibatch:

$$\Delta\theta_k = -\epsilon_k \nabla_{\theta=\theta_{k-1}} \left( \frac{|\mathcal{D}|}{|\tilde{\mathcal{D}}|} \mathcal{L}(\theta, \tilde{\mathcal{D}}) + \psi(\theta) \right) + \sqrt{2\epsilon_k} z_k, \quad (3)$$

where  $\tilde{\mathcal{D}} \subseteq \mathcal{D}$  is a fixed size minibatch, for which data points are sampled uniformly at random from  $\mathcal{D}$  with replacement. We will refer to this algorithm as *Langevin SGD*.

Note that the first term in Equation 3 is an unbiased estimator of the first term in Equation 2. Welling and Teh (2011) argue that, for an appropriately chosen step size sequence, the marginal distribution of  $\theta_k$  converges to the posterior distribution in a sense that can be made precise.

To introduce notation that simplifies development of Langevin DQN, let  $\alpha_k = \epsilon_k |\mathcal{D}|$  so that we can rewrite Langevin SGD (3) as

$$\Delta\theta_k = -\alpha_k \nabla_{\theta=\theta_{k-1}} \left( \frac{\mathcal{L}(\theta, \tilde{\mathcal{D}})}{|\tilde{\mathcal{D}}|} + \frac{\psi(\theta)}{|\mathcal{D}|} \right) + \sqrt{\frac{2\alpha_k}{|\mathcal{D}|}} z_k. \quad (4)$$

### 3. Reinforcement Learning

Langevin DQN synthesizes Langevin SGD and DQN to address RL. In this paper, we restrict attention to an episodic RL setting in which an agent interacts with an unknown environment over episodes, aiming to maximize accumulated rewards. We model the environment as a Markov Decision Process (MDP) characterized by a quintuple  $\mathcal{M} = (\mathcal{S}, \mathcal{A}, \mathcal{R}, \mathcal{P}, \rho)$ . Here,  $\mathcal{S}$  is a finite state space,  $\mathcal{A}$  is a finite action space,  $\mathcal{R}$  is a reward model,  $\mathcal{P}$  is a transition model, and  $\rho$  is an initial state distribution. Given a state  $s \in \mathcal{S}$ , action  $a \in \mathcal{A}$ , and next state  $s' \in \mathcal{S}$ ,  $\mathcal{R}_{s,a,s'}(\cdot)$  denotes a distribution of the possible rewards the agent can experience when transitioning from  $s$  to  $s'$  upon taking action  $a$ . Similarly,  $\mathcal{P}_{s,a}(s')$  is the conditional probability that the state

transitions to  $s'$  from state  $s$  upon taking action  $a$ , while  $1 - \sum_{s' \in \mathcal{S}} \mathcal{P}_{s,a}(s')$  is the probability that the episode terminates. We denote the sequence of observations made by the agent in episode  $l$  by  $(s_0^l, a_0^l, r_0^l, s_1^l, \dots, s_{\tau^l-1}^l, a_{\tau^l-1}^l, r_{\tau^l-1}^l, s_{\tau^l}^l)$ , where  $s_h^l$  is the state of the environment observed by the agent at time  $h$  and episode  $l$ ,  $r_h^l$  is the reward observed by the agent on taking an action  $a_h^l$ , and  $\tau^l$  denotes the time at which episode terminates at state  $s_{\tau^l}^l$ .

A (stationary stochastic) policy  $\pi : \mathcal{S} \times \mathcal{A} \rightarrow [0, 1]$  assigns to each state a probability mass function over actions. In particular, we denote by  $\pi(a|s)$  the probability that the policy selects action  $a$  when in state  $s$ . Let  $\Pi$  denote the set of all policies. Denote by  $P_\pi$  the transition probability matrix under policy  $\pi$ ; i.e.,  $P_{\pi,s,s'} = \sum_{a \in \mathcal{A}} \pi(a|s) \mathcal{P}_{s,a}(s')$ . We make the following assumption, which ensures that episodes terminate.

**Assumption 1.** (*finite episodes*)  
For all  $\pi \in \Pi$ ,  $\lim_{h \rightarrow \infty} P_\pi^h = 0$ .

Under Assumption 1, the state-action value function  $Q^\pi : \mathcal{S} \times \mathcal{A} \mapsto \mathfrak{R}$  of each policy  $\pi$  is defined by

$$Q^\pi(s, a) = \mathbb{E}_{\mathcal{M}, \pi} \left[ \sum_{h=0}^{\tau-1} r_h \mid s_0 = s, a_0 = a \right],$$

where the subscripts of the expectation indicate that state transitions and rewards are generated by MDP  $\mathcal{M}$  with actions sampled by policy  $\pi$ . We denote the optimal value function by  $Q^*(s, a) = \max_{\pi \in \Pi} Q^\pi(s, a)$

Similarly with DQN, Langevin DQN, is a value learning algorithm. In value learning, an agent updates the parameter vector  $\theta$  of a parameterized value function  $Q_\theta$  as data accumulates, with an aim of estimating the optimal value function  $Q^*$ . At each time, an action is selected based on the current value function estimate.

A template for value learning with greedy actions is presented in Algorithm 1. The algorithm begins with an empty data buffer and then iterates over episodes. In each episode, the agent updates the parameter vector based on buffered data and then applies  $\epsilon$ -greedy actions through termination. The parameter update could be carried out, for example, by the DQN or Langevin DQN algorithm. These algorithms makes use of a target model with parameter vector  $\theta^{\text{target}}$  in their updates to maintain stability (Mnih et al., 2015).  $\theta^{\text{target}}$  is a snapshot of  $\theta$  and updated periodically (say, every  $M$  episodes). Observed actions, state transitions, and rewards are added to the buffer. In particular, each item in the buffer is a tuple  $(s, a, r, s')$ , where  $s$  is a state,  $r$ ,  $s'$  are the reward and the next state observed by the agent on taking an action  $a$ . The most basic version of a buffer would simply accumulate all observations. But in practical implementations, one might design a discipline that limits the buffer size by ejecting old or randomly selected data samples.

## 4. Langevin DQN

The DQN algorithm updates the parameter vector  $\theta$  by taking SGD-like steps that aim to reduce TD loss possibly summed with a regularization penalty. These SGD-like steps are similar to Algorithm 2, but without the Gaussian noise term. The Langevin DQN update, presented in Algorithm 2 instead uses Langevin-SGD-like steps.

---

**Algorithm 1** greedy\_value\_rl

---

**Input:**  $\theta_0$  initial parameters  
 $Q_\theta(s = \cdot, a = \cdot)$  parameterized value function  
 $\epsilon$  exploration intensity  
 $M$  target update frequency

- 1:  $\theta^{\text{target}} \leftarrow \theta_0$
- 2:  $\text{buffer} \leftarrow \text{Buffer.init}()$
- 3: **for** episode  $l = 1, 2, \dots$  **do**
- 4:  $\theta \leftarrow \text{update}(\text{buffer}, \theta, \theta^{\text{target}})$
- 5: **if**  $M \mid l$  **then**
- 6:  $\theta^{\text{target}} \leftarrow \theta$
- 7: **end if**
- 8:  $h \leftarrow 0$
- 9: observe  $s_0^l$
- 10: **while**  $s_h^l$  is not terminal **do**
- 11: apply 
$$a_h^l \leftarrow \begin{cases} \text{unif}(\arg \max_a Q_\theta(s_h^l, a)) & \text{w.p. } 1 - \epsilon \\ \text{unif}(\mathcal{A}) & \text{w.p. } \epsilon \end{cases}$$
- 12: observe  $r_h^l, s_{h+1}^l$
- 13:  $\text{buffer.add}((s_h^l, a_h^l, r_h^l, s_{h+1}^l))$
- 14:  $h \leftarrow h + 1$
- 15: **end while**
- 16: **end for**

---

---

**Algorithm 2** LangevinDQN\_update

---

**Input:**  $\mathcal{L}(\theta = \cdot; \theta^{\text{target}} = \cdot, \mathcal{D} = \cdot)$  TD loss  
 $\psi(\theta = \cdot)$  regularizer  
 $\alpha$  learning rate  
 $\mathcal{D}$  data buffer  
 $B$  mini-batch size  
 $\theta^-$  parameters  
 $\theta^{\text{target}}$  target parameters

**Return:**  $\theta^+$  new parameters

- 1:  $\tilde{\mathcal{D}} \leftarrow \text{sample\_minibatch}(\mathcal{D}, B)$
- 2:  $z \leftarrow \text{sample\_normal}(0, I_{\dim(\theta^-)})$
- 3: compute increment

$$\Delta\theta \leftarrow -\alpha \nabla_{\theta=\theta^-} \left( \frac{1}{|\tilde{\mathcal{D}}|} \mathcal{L}(\theta, \theta^{\text{target}}, \tilde{\mathcal{D}}) + \frac{1}{|\mathcal{D}|} \psi(\theta) \right) + \sqrt{\frac{2\alpha}{|\mathcal{D}|}} z \quad (5)$$

- 4: return  $\theta^- + \Delta\theta$

---

For a buffer  $\mathcal{D}$  with elements of form  $(s, a, r, s')$ , the TD loss used in algorithm 2 can be written as

$$\mathcal{L}(\theta, \theta^{\text{target}}, \mathcal{D}) = \sum_{(s, a, r, s') \in \mathcal{D}} \mathcal{L}(\theta, \theta^{\text{target}}, (s, a, r, s')),$$

where

$$\mathcal{L}(\theta, \theta^{\text{target}}, (s, a, r, s')) = \frac{1}{2\sigma_w^2} (r + \max_{a' \in \mathcal{A}} Q_{\theta^{\text{target}}}(s', a') - Q_{\theta}(s, a))^2,$$

with an understanding that  $Q_{\theta}(s', a') = 0$  if the transition from  $s$  terminates the episode. The term that is squared in this expression is the so-called *temporal difference*.

Langevin DQN is very similar to DQN, requiring very minor changes. The primary difference lies in the fact that, while Langevin DQN updates parameters based on an expression very similar to DQN, the expression used in Langevin DQN includes an additional random perturbation term. The only other difference is that, while  $\epsilon$ -greedy exploration is typically used with DQN, Langevin DQN needs no additional exploration scheme and thus it suffices to apply greedy actions. We would like to note that it is possible to design reinforcement learning algorithms that operate in continuing rather than episodic environments using an update rule similar to Langevin DQN, though we do not develop that idea here.

## 5. Computational Results

To assess whether Langevin DQN achieves deep exploration, we apply it to the deep sea environment (Osband et al., 2019, 2020). The deep sea environment with depth  $N$  can be seen as an  $N \times N$  two-dimensional grid in which the agent starts in the upper-right corner and should ideally reach a treasure chest located at the lower-left corner as shown in Figure 1.

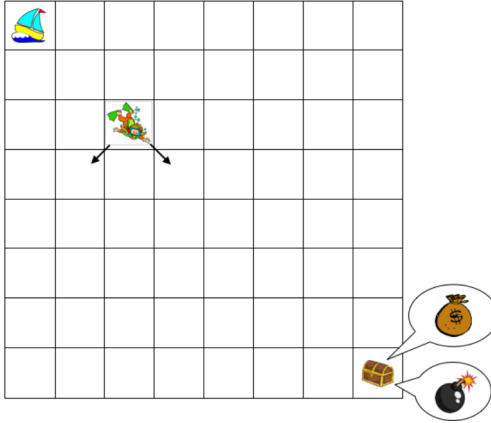


Figure 1: Deep sea environment (Osband et al., 2019)

At each time, the agent applies an action from  $\mathcal{A} = \{0, 1\}$  to move to the left or to the right cell in the next row. However, the mapping between  $\{0, 1\}$  to  $\{left, right\}$  is unknown to the agent and varies across states. For simplicity, we assume that there is a treasure in the chest, which is revealed

to the agent when it takes the *right* action on reaching the chest, resulting in a reward of 1. In addition there is a small penalty of  $0.01/N$  whenever the agent takes the *right* action.

We compare the performance of Langevin DQN against traditional DQN (Mnih et al., 2013), which uses  $\epsilon$ -greedy exploration. Both share Algorithm 1 as a template. Recall that Langevin DQN agent acts greedily according to its value function estimates which is obtained by applying iterations of Algorithm 2 in the update step in Algorithm 1.

In our experiments, we use neural networks to approximate value functions. Langevin DQN and DQN each use a single neural network mapping state-action pairs to value. We use common hyperparameters, including neural network, buffer discipline, buffer size, batch size, number of updates performed between episodes, and target network update frequency, for both algorithms. This ensures that update routines impose similar computational requirements. The learning rate sequence was tuned separately to optimize the performance of each algorithm. The exploration intensity  $\epsilon$  was set to zero for Langevin DQN but tuned to optimized performance for DQN.

We used the Adam optimizer (Kingma and Ba, 2014) for updating parameters of DQN. Since Langevin DQN has an additional random perturbation term in the update equation, Adam could not be used in a straightforward manner. Hence, we implemented preconditioned SGLD (Li et al., 2016), using the Adam optimizer as the backbone. It is worth noting that we also tried implemented both algorithms with the classical stochastic gradient descent optimizer; however, the performance was significantly worse in both cases than with an adaptive step size optimizer. The exact values of hyperparameters used in our experiments are provided in the appendix.

In order to assess and compare performance, we define a notion of learning time. In particular, we take learning time to be the first episode at which cumulative regret is less than 0.9 times the number of episodes. In other words,

$$\text{learning time} = \min\{l : \text{Regret}(l) < 0.9l\}.$$

The cumulative regret until the episode  $l$  is defined as the difference between the maximal reward that the agent could have accumulated and the reward that the agent has accumulated over the  $l$  episodes. In the case of the deep sea environment, the maximum possible reward an agent can obtain in an episode is 0.99, and the agent observes a positive reward only when it takes the optimal actions throughout the episode and reaches the treasure chest. In all other cases, the agent observes a non-positive reward and experiences regret of at least 0.99. The learning time can be thought of as the first episode by which the agent has behaved optimally for at least a tenth of past episodes.

It is easy to establish a lower bound on the median learning time of dithering exploration schemes like  $\epsilon$ -greedy for the deep sea environments, irrespective of the exploration intensity  $\epsilon$ . When the agent starts with an uninformative value function, the agent needs to reach the treasure chest to learn the optimal value function. Let us ignore the penalty of  $-0.01/N$  on taking the *right* action. Let  $l^*$  be the first episode at which the agent reaches the treasure chest. Under the  $\epsilon$ -greedy strategy, for any episode before  $l^*$ , all actions are sampled uniformly at random. Thus, the probability of reaching the treasure is  $1/2^N$ . Hence,  $l^*$  is a geometric random variable with the probability of success as  $1/2^N$ . If we account for the penalty for taking the *right* action, the probability of success becomes even lower. Thus, the median learning time  $E[l^*]$  for an  $\epsilon$ -greedy strategy is lower bounded by  $2^N$ . We can calculate the lower bounds on other percentiles as the percentiles of the Geometric( $1/2^N$ ) random variable.

We carried out experiments with deep sea environments with depths varying from 3 to 30 in multiples of 3. In each trial, an agent operated over 10,000 episodes. For DQN agent, we experimented with different values of  $\epsilon$  and found that starting with a value of 0.2 and decaying it

with the number of episodes optimized performance. We tuned over the choice of learning rate,  $\sigma_w^2$  and  $\sigma_p^2$  for each of the algorithms separately, finding that  $\sigma_w = 0.01$  and  $\sigma_p = 1$  seems to lead to the best results for both algorithms. For each set of hyperparameters, we ran 5 trials, each with a different random seed. Note that as the depth of the deep sea increases, more data accumulates per episode. Since we used a fixed mini-batch size, we scaled the number of update steps by the depth of the deep sea environment in both Langevin DQN and DQN algorithms.

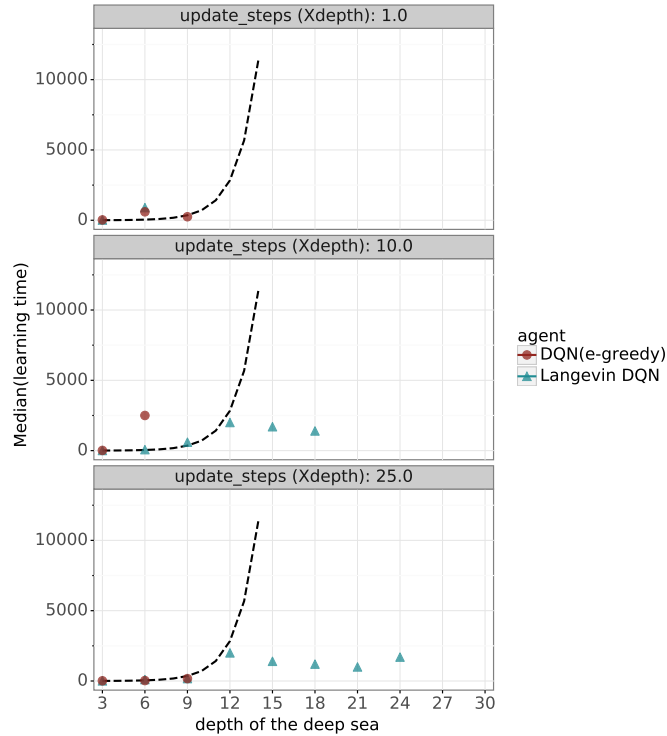


Figure 2: Median learning times of Langevin DQN vs.  $\epsilon$ -greedy DQN. Lower the learning times imply better performance. The dashed curve is a theoretical lower bound on the median learning time of the  $\epsilon$ -greedy strategy. Experiments were carried out with each algorithm on environments with depths of multiples of 3 for 10,000 episodes. Where data is not plotted, the algorithm failed to learn the optimal policy, in at least half of the trials.

Figure 2 compares the median learning times of Langevin DQN versus  $\epsilon$ -greedy DQN across different environment depths. If the agent was not able learn an optimal policy within 10,000 episodes, we consider the agent to have failed. If the agent fails across more than half the random seeds, data is omitted from the plot. We take the median of the learning times instead of the mean to make results robust to failures. We also provide plots comparing the median learning times across different numbers of update steps per episode. The dashed curve in the plots represents the theoretical lower bound on the median learning time for an  $\epsilon$ -greedy agent. We observe that as the

number of update steps per an episode increases, Langevin DQN is capable of learning in deeper environments. Note that DQN fails for environments with depth greater than 9.

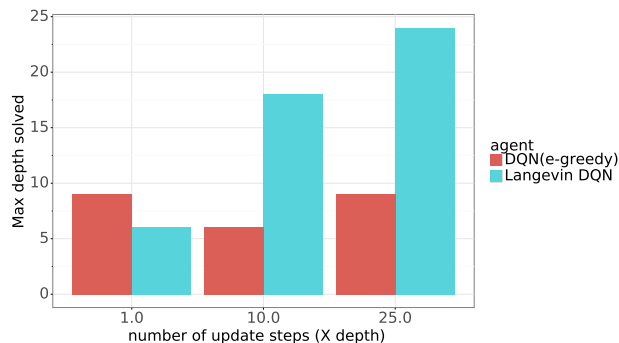


Figure 3: Maximum depth solved by at least half of the trials for Langevin DQN vs.  $\epsilon$ -greedy DQN.

Figure 3 plots the maximum depth of the environments that were solved across at least half of the trials by Langevin DQN and DQN, across different numbers of update steps. Since the learning time of DQN stochastically dominates Geometric( $1/2^N$ ) random variable, it takes more than  $2^N$  episodes to observe a reward in at least half of the trials of  $\epsilon$ -greedy DQN. As we are testing the algorithms for 10000 episodes, DQN cannot solve an environment of depth greater than 13 with a non-negligible probability. However, as shown in Figure 3, Langevin DQN solves an environment of depth 24. From this plot we can see that Langevin DQN algorithm is capable of solving deeper deep sea environments as we increase the number of update steps. This verifies that Langevin DQN algorithm achieves *deep exploration*. However, for any value of  $\epsilon \in [0, 1]$ ,  $\epsilon$ -greedy DQN would require at least  $1.6 \times 10^7$  to achieve a similar performance! This demonstrates that DQN can not handle deep environments regardless of the number of update steps while Langevin DQN is capable of deep exploration.

Figure 2 demonstrated Langevin DQN succeeding in environments of depth up to 24. Figure 3 suggests that this depth can scale with update steps. It is also interesting to study Figure 4, which plots twentieth percentile instead of median learning times. These plots indicates that even with the number of update steps we applied, Langevin DQN sometimes solves environments of depth up to 30 or beyond. DQN, on the other hand, exhibits failing behavior predicted by the theoretical lower bound.

It is important to note that the bottleneck for Langevin DQN algorithm is computational and not statistical. From Figure 3, we can see that Langevin DQN algorithm solves deeper environments as we allocate more compute cycles to perform more update steps. On the other hand, the bottleneck for DQN algorithm with  $\epsilon$ -greedy is statistical. In particular, allocating more compute cycles to DQN algorithm, does not enable it to solve deeper environments.

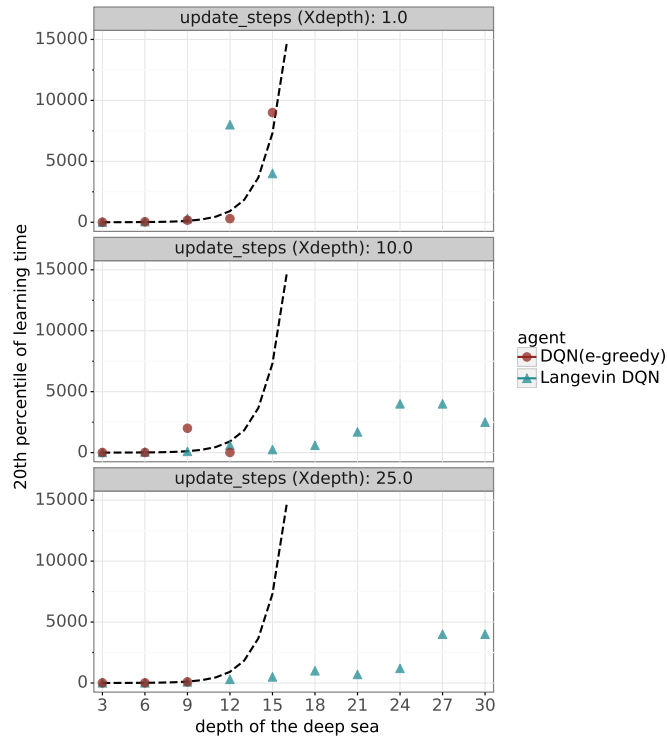


Figure 4: Twentieth percentile learning times of Langevin DQN vs.  $\epsilon$ -greedy DQN. The dashed curve is a theoretical lower bound on the twentieth percentile learning time of the  $\epsilon$ -greedy strategy. Experiments were carried out with each algorithm on environments with depths of multiples of 3 for 10,000 episodes. Where data is not plotted, the algorithm failed to learn the optimal policy in all trials.

## 6. Why Langevin DQN Works

In this section, we offer some insight into why Langevin DQN achieves deep exploration by perturbing parameter updates. We consider a simple example (adapted from Section 5.3.2, Osband et al. 2019) to understand the role of the perturbation and how it induces deep exploration.

To illustrate how Langevin DQN performs deep exploration, we consider a fixed horizon MDP  $M$  with four states  $\mathcal{X} = \{1, 2, 3, 4\}$ , two actions  $\mathcal{A} = \{up, down\}$  and a horizon of  $H = 6$ . Let  $\mathcal{D}$  be the list of all transitions observed so far, and let  $\mathcal{D}_{x,a} = \{(\hat{x}, \hat{a}, r, x') \in \mathcal{D} : (\hat{x}, \hat{a}) = (x, a)\}$  contain the transitions from state-action pair  $(x, a)$ . Suppose  $|\mathcal{D}_{4,down}| = 1$ , while for every other state-action pair  $(x, a) \neq (4, down)$ ,  $|\mathcal{D}_{x,a}|$  is very large, virtually infinite. Hence, we are highly uncertain about the expected immediate rewards for and transition probabilities of taking action *down* at state 4. Assume that this is the case for all time periods  $h \in \{0, 1, \dots, 5\}$ .

Let  $Q_h^*$  denote the  $Q^*$  value at time  $h$ . Since we are uncertain about the MDP  $\mathcal{M}$ ,  $Q_h^*$  is a random vector. Figure 5 illustrates our uncertainty in these quantities. Each triangle in row  $x$  and column  $h$  contains two smaller triangles that are associated with  $Q_h^*$ -values of *up* and *down*

actions at state  $x$ . The shade on the smaller triangle shows the uncertainty in the  $Q_h^*(x, a)$ . Here, we consider variance as the measure of uncertainty. The dotted lines indicate plausible transitions, except at  $(4, \text{down})$ . Since we are uncertain about  $(4, \text{down})$ , any transition is plausible.

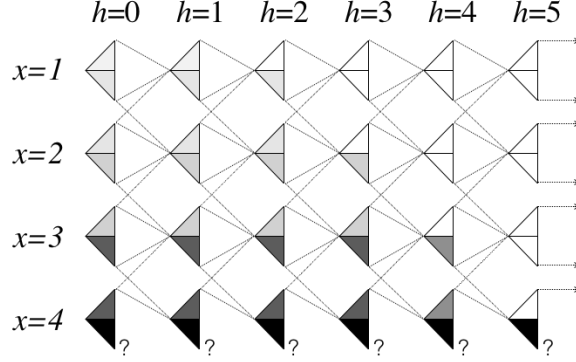


Figure 5: Example to illustrate how Langevin DQN achieves deep exploration

At  $h = H - 1 = 5$ , since  $Q_5^*$  is only affected by the immediate rewards, the only uncertain quantity is  $Q_5^*(4, \text{down})$ . If we move one step back to  $h = 4$ , we are highly uncertain about  $Q_4^*(4, \text{down})$  and slightly uncertain about  $Q_4^*(3, \text{down})$  and  $Q_4^*(4, \text{up})$ . This is because of the propagation of uncertainty from  $(4, \text{down})$  at  $h = 5$  to  $(3, \text{down})$  and  $(4, \text{up})$  at  $h = 4$ . The uncertainty propagates backward in time which can be visualized as progressing leftward in Figure 5. Specifically, we can see that the uncertainty in  $Q_5^*(4, \text{down})$  can even influence the uncertainty in  $Q_0^*(1, \text{up})$ .

Now, let us look at samples  $Q_{\hat{\theta}_h^k}(x, a)$  generated by Langevin DQN after the  $k$  update steps of (5) with  $\alpha = \epsilon|\mathcal{D}|$  and  $\theta^{\text{target}}$  as the current estimate of  $\theta$ . Here, we provide an argument for why the variance of  $Q_{\hat{\theta}_h^k}(x, a)$ , tends to grow and shrink with the variance of  $Q_h^*(x, a)$ . For simplicity, let the entire buffer be used instead of a mini-batch,  $\psi$  be 0, and a tabular representation be used for the value functions. In particular, parameter vector  $\theta$  is the concatenation of  $\theta_0, \theta_1, \dots, \theta_5 \in \mathbb{R}^{|\mathcal{X}| \times |\mathcal{A}|}$ , and each component of  $\theta_h$  encodes the value  $Q_{\theta_h}(x, a)$  of a single state-action pair  $(x, a)$  at time  $h$ . From these assumptions, the update equation (5) at the  $k$ th iteration is given by

$$Q_{\hat{\theta}_h^k}(x, a) = Q_{\hat{\theta}_{h-1}^k}(x, a) - \epsilon \frac{1}{\sigma_w^2} \sum_{(\tilde{x}, \tilde{a}, r, x') \in \mathcal{D}_{x,a}} \left( Q_{\hat{\theta}_{h-1}^k}(\tilde{x}, \tilde{a}) - r - \max_{a' \in \mathcal{A}} Q_{\hat{\theta}_{h-1}^k}(x', a') \right) + \sqrt{2\epsilon} z_h^k \quad (6)$$

with  $Q_{\theta_6}(x, a) = 0 \forall x \in \mathcal{X}, a \in \mathcal{A}$ .

Note that if  $|\mathcal{D}_{x,a}|$  is large, the perturbation term is dominated by the loss term and  $Q_{\hat{\theta}_h^k}(x, a)$  remaining almost unchanged and close to  $\mathbb{E}[r_{t+1} + \max_{a' \in \mathcal{A}} Q_{\hat{\theta}_{h-1}^k}(x_{h+1}, a') | x_h = x, a_h = a]$ . This is true for all state-action pairs except  $(4, \text{down})$ . Because  $|\mathcal{D}_{4, \text{down}}| = 1$ , the value of  $Q_{\hat{\theta}_h^k}(4, \text{down})$  will exhibit high variation.

From (6), for each state-action pair  $(x, a)$ , the sequence  $Q_{\theta_0}(x, a), Q_{\theta_1}(x, a), \dots$  can be seen as a Markov chain. At  $h = 5$ ,  $Q_{\hat{\theta}_5^k}(x, a)$  is highly concentrated around  $Q_5^*(x, a)$  for all  $(x, a) \neq (4, \text{down})$ , and  $Q_{\hat{\theta}_5^k}(4, \text{down})$  will have high variance. At  $h = 4$ ,  $Q_{\hat{\theta}_4^k}(4, \text{up})$  and  $Q_{\hat{\theta}_4^k}(3, \text{down})$  also start

exhibiting variance after a few updates because of the propagation of uncertainty from  $Q_{\hat{\theta}_5^k}^*(4, \text{down})$ . Working backward in time, leftward in Figure 5, we can see that the uncertainty propagates backward, as shown by the shaded areas in the triangles.

The update equation (6), can be seen as a discretized version of a SDE

$$dQ_{\hat{\theta}_h^t}(x, a) = -\frac{1}{\sigma_w^2} \sum_{(\tilde{x}, \tilde{a}, r, x') \in \mathcal{D}_{x,a}} \left( Q_{\hat{\theta}_h^t}(\tilde{x}, \tilde{a}) - r - \max_{a' \in \mathcal{A}} Q_{\hat{\theta}_{h+1}^t}(x', a') \right) dt + \sqrt{2} dB_h^t,$$

where  $B_h^t$  is a standard Brownian motion in  $\mathbb{R}^d$ . This SDE can also help us understand the uncertainty propagation. The uncertainty in  $Q_{\hat{\theta}_5}(4, \text{down})$  contributes to the uncertainty in  $Q_{\hat{\theta}_4}(3, \text{down})$  and  $Q_{\hat{\theta}_4}(4, \text{up})$  as the rest of the values of  $Q_{\hat{\theta}_5}$  are concentrated. As we go backward in time, the uncertainty propagates as shown by the shaded triangles in Figure 5.

This uncertainty drives exploration. A high variance in  $Q_{\hat{\theta}_h}(x, a)$  generates optimistic  $Q_{\hat{\theta}_h}(x, a)$  in some episodes, incentivizing the agent to try those actions. Note that the uncertainty in the state-action value exists not only because of the uncertainty in the immediate reward and transitions but also from the propagation of the uncertainty from multiple time periods. This process leads to deep exploration.

Note that the main advantage of the Langevin DQN is its simplicity. In spite of being very similar to DQN, the Langevin DQN algorithm is capable of deep exploration.

## 7. Conclusion

In this paper, we introduced Langevin DQN, a slight variation of DQN that achieves deep exploration using a single point estimate of the value function. We demonstrated this through computational experiments and provided insights into how Langevin accomplishes this.

## References

- Xiang Cheng, Niladri S Chatterji, Yasin Abbasi-Yadkori, Peter L Bartlett, and Michael I Jordan. Sharp convergence rates for Langevin dynamics in the nonconvex setting. *arXiv preprint arXiv:1805.01648*, 2018.
- Vikranth Dwaracherla, Xiuyuan Lu, Morteza Ibrahimi, Zheng Osband, Ian Oand Wen, and Benjamin Van Roy. Hypermodels for exploration. In *International Conference on Learning Representations*, 2020.
- Vikranth R Dwaracherla, Benjamin Van Roy, and Morteza Ibrahimi. Posterior sampling networks. In *Reinforcement Learning and Decision Making Conference*, pages 366–370, 2019.
- Meire Fortunato, Mohammad Gheshlaghi Azar, Bilal Piot, Jacob Menick, Matteo Hessel, Ian Osband, Alex Graves, Volodymyr Mnih, R/emi Munos, Demis Hassabis, Olivier Pietquin, Charles Blundell, and Shane Legg. Noisy networks for exploration. In *International Conference on Learning Representations*, 2018.
- Diederik P Kingma and Jimmy Ba. Adam: A method for stochastic optimization. *arXiv preprint arXiv:1412.6980*, 2014.

- Chunyu Li, Changyou Chen, David Carlson, and Lawrence Carin. Preconditioned stochastic gradient Langevin dynamics for deep neural networks. In *Thirtieth AAAI Conference on Artificial Intelligence*, 2016.
- Xiuyuan Lu and Benjamin Van Roy. Ensemble sampling. In *Advances in Neural Information Processing Systems*, pages 3258–3266, 2017.
- Volodymyr Mnih, Koray Kavukcuoglu, David Silver, Alex Graves, Ioannis Antonoglou, Daan Wierstra, and Martin Riedmiller. Playing Atari with deep reinforcement learning. *arXiv preprint arXiv:1312.5602 - NIPS Deep Learning Workshop*, 2013.
- Volodymyr Mnih, Koray Kavukcuoglu, David Silver, Andrei A Rusu, Joel Veness, Marc G Bellemare, Alex Graves, Martin Riedmiller, Andreas K Fidjeland, Georg Ostrovski, et al. Human-level control through deep reinforcement learning. *Nature*, 518(7540):529–533, 2015.
- I. Osband, D. Russo, and B. Van Roy. (More) efficient reinforcement learning via posterior sampling. In *Advances in Neural Information Processing Systems 26*. Curran Associates, Inc., 2013.
- Ian Osband, Charles Blundell, Alexander Pritzel, and Benjamin Van Roy. Deep exploration via bootstrapped DQN. In *Advances in Neural Information Processing Systems*, pages 4026–4034, 2016.
- Ian Osband, John Aslanides, and Albin Cassirer. Randomized prior functions for deep reinforcement learning. In *Advances in Neural Information Processing Systems*, pages 8626–8638, 2018.
- Ian Osband, Daniel Russo, Zheng Wen, and Benjamin Van Roy. Deep exploration via randomized value functions. *Journal of Machine Learning Research*, 20(124):1–62, 2019.
- Ian Osband, Yotam Doron, Matteo Hassel, John Aslanides, Eren Sezener, Andre Saraiva, Katrina Mckinney, Tor Lattimore, Csaba Szepesvari, Satinder Singh, Benjamin Van Roy, Richard Sutton, David Silver, and Hado Van Hasselt. Behaviour suite for reinforcement learning. In *International Conference on Learning Representations*, 2020.
- Grigorios A Pavliotis. *Stochastic processes and applications: diffusion processes, the Fokker-Planck and Langevin equations*, volume 60. Springer, 2014.
- Daniel J Russo, Benjamin Van Roy, Abbas Kazerouni, Ian Osband, Zheng Wen, et al. A tutorial on Thompson sampling. *Foundations and Trends® in Machine Learning*, 11(1):1–96, 2018.
- William R Thompson. On the likelihood that one unknown probability exceeds another in view of the evidence of two samples. *Biometrika*, 25(3/4):285–294, 1933.
- Max Welling and Yee W Teh. Bayesian learning via stochastic gradient Langevin dynamics. In *Proceedings of the 28th international conference on machine learning (ICML-11)*, pages 681–688, 2011.

## Appendix A. Hyperparameters used in the experiments

Neural networks were used to approximate the  $Q$ -values in our experiments. Bsuite (Osband et al., 2020) code base was used to build and test the Langevin DQN and  $\epsilon$ -greedy DQN algorithms on the deep sea environment. The state of the deep sea environment is encoded as a one hot vector and passed as an input to the neural network. This neural network had 2 outputs, corresponding to the 2 possible actions, had 2 hidden layers with 50 ReLU units in each layer for both the algorithms. A target network with the exact same architecture as the  $Q$ -value network is used, whose weights are set to the weights of the  $Q$ -value network every few episodes. The hyperparameters which are common for both the algorithms are:

hyperparameter	value
mini-batch size	128
buffer size	$10^5$
learning rate	$2 \times 10^{-4} \sigma_w^2$
$\sigma_w$	0.01
$\sigma_p$	1.0
target update frequency	5 episodes

We ran 5 trials on each set of hyperparameters, each of these trials was set a random seed from 0 to 4 for both the algorithms. A FIFO buffer of finite size was used. The Adam optimizer was used for updating parameters in the DQN algorithm, and the preconditioned SGD (Li et al., 2016), with the Adam optimizer as the backbone, was used for the Langevin DQN algorithm. For both the algorithms, we initially tested the hyperparameters on smaller deep sea environments and then deployed the optimal set of hyperparameters for all deep sea environments. We used a constant learning rate and tested different values of learning rate from  $[10^{-5}, 10^{-2}] \sigma_w^2$  and found that  $2 \times 10^{-4} \sigma_w^2$  gives the best performance. We have also experimented with different values of  $\sigma_w$  from  $[0.001, 1.0]$ , both the algorithms perform significantly better when  $\sigma_w$  is around 0.01. We also tuned over the target update frequency from  $\{3, 5, 10, 25, 100\}$  and 5, 10 seems to give the best performance with 5 being marginally better. For the  $\epsilon$ -greedy DQN algorithm, we tuned  $\epsilon$  from  $[0.01, 0.25]$  and experimented with and without a decay in the exploration intensity. The value of exploration intensity as  $\epsilon g / (g + \text{number of data points accumulated})$  with  $\epsilon = 0.2$ ,  $g = 1000$  worked the best.

We also found that modifying the (5) by replacing  $\sqrt{\frac{2\alpha}{|\mathcal{D}|}}z$  with  $\sqrt{\frac{2\alpha g}{g+|\mathcal{D}|}}z$ ,  $g = 50$  gave an improvement in the performance when a very low number of update steps were used to update the parameters of the Langevin DQN algorithm. This helps in slowing down the rate at which the perturbation decreases (perturbation term decreases as the buffer  $\mathcal{D}$  grows), helping the Langevin DQN algorithm to explore more.